Effects of Na/Ti ratio on the properties of sodium titanate for photocatalytic degradation of ofloxacin

Shengwei Chen, Wenjie Zhang*, Chang Ye

*School of Environmental and Chemical Engineering, Shenyang Ligong University, Shenyang 110159, China,
emails: wjzhang@aliyun.com (W. Zhang), 3215131398@qq.com (S. Chen), 1872067390@qq.com (C. Ye)*

ABSTRACT

A sol–gel method was applied to prepare sodium titanate samples with different Na/Ti molar ratios, that is, $n(Na)/n(Ti)$ = 2:3 (Na_2Ti_3), 2:6 (Na_2Ti_6) and 2:9 (Na_2Ti_9). Nano-sized $Na_2Ti_6O_{13}$ was the main substance in all the samples, while Na_2Ti_3 contained a minor proportion of $Na_4Ti_5O_{12}$, and rutile phase TiO_2 was a minor component in Na_2Ti_9. The adsorption–desorption isotherms of the samples were regarded as an International Union of Pure and Applied Chemistry Type IV isotherm for mesoporous materials. The band gap energies for Na_2Ti_3, Na_2Ti_6 and Na_2Ti_9 were calculated to be 3.28, 3.15 and 3.06 eV, respectively. The productivity of hydroxyl radicals on the sodium titanates was in the sequence $Na_2Ti_9 > Na_2Ti_6 > Na_2Ti_3$. The original ofloxacin molecules were nearly completely degraded after 70 min of reaction in the presence of Na_2Ti_6 and Na_2Ti_9, while the degradation efficiency was only 54.7% for Na_2Ti_3. The reaction rate constants for ofloxacin degradation occurred on Na_2Ti_3, Na_2Ti_6 and Na_2Ti_9 were calculated to be 0.00693, 0.0154 and 0.0187 min⁻¹, respectively. A total of 88.1% of the original activity of Na_2Ti_6 was maintained in the fifth reaction cycle.

Keywords: Photocatalytic; Sodium titanate; Degradation; Ofloxacin

1. Introduction

Antibiotics are annually produced and applied in a large amount. The wastewater discharged from antibiotics producers usually contains a significant concentration of antibiotics. The wastewater must be purified to remove the antibiotics before discharging. However, the antibiotics polluted wastewater is hard to be removed in the traditional bio-chemical treatment plant, since the antibiotics are harmful to microorganisms [1–3]. Special techniques are needed to deal with such kind of hazardous wastewater, for example, photocatalytic technique [4–6]. Ofloxacin and chlortetracycline were reported to degrade during the photocatalytic oxidation processes [7–9].

The investigations in photocatalysts were essential to the developments of photocatalytic technique [10–12]. TiO_2 was used as a basic material in this research field. Titanates were frequently reported in the recent literatures, and some kinds of titanates were the potential materials for wastewater treatment [13–16]. Tavasol et al. [17] designed sea sediment/titanate to purify cephalexin antibiotic solution. Liu et al. [18] reported antibiotic degradation on bismuth titanate. We reported the degradation of ofloxacin on a $Sm_2Ti_2O_7/n$HZSM-5 composite [19].

Sodium titanate was known as a typical dielectric material [20,21]. The recent literatures revealed the application of sodium titanates in the photocatalytic reactions. Shi et al. [22] prepared sodium titanate necklaces to study oxygen vacancies and photocatalytic activity. Shtyka et al. [23] synthesized mixed-phase sodium titanates for visible-light driven reduction of carbon dioxide. Wang et al. [24] prepared a sodium titanate nanosheet encapsulated *p-n* heterojunction photocatalyst. However, sodium titanate is still a new type of photocatalyst, and the application of sodium titanate on

* Corresponding author.

the removal of organic pollutants is interesting. There was no literature reporting the degradation of antibiotics on sodium titanate.

A sol–gel method was applied to prepare sodium titanate in this work. The composition of the precursor was changed to adjust the molar ratio of sodium/titanium. The properties of the obtained sodium titanates were investigated using different characterization techniques, and the application of the sodium titanates was studied in an ofloxacin degradation process. The main finding of this work was the influences of sodium/titanium molar ratio on the composition and properties of the sodium titanate samples, especially on the performance in the photocatalytic degradation of ofloxacin.

2. Experimental methods

2.1. Sodium titanate preparation

Ethanol (16 mL) and tetrabutyl titanate (0.005 mol) were used to prepare solution I. Sodium acetate was dissolved in pure water (15 mL), and then acetic acid (16 mL) was added to form solution II. Solution I, solution II and glycol (2 mL) were stirred together to obtain a sol. The sol–gel process was accomplished in an 80°C water bath. After 18 h of dehydration of the gel at 110°C, the subsequent thermal treatment was conducted at 700°C for 3 h. The products were ground before use. Table 1 gives the sodium titanates prepared with different n(Na)/n(Ti) ratios.

2.2. Characterization of sodium titanate samples

The phase compositions of the sodium titanate samples were obtained using a D8 X-ray diffractometer (Cu Kα, 0.1542 nm). The scanning electron photos of the materials were obtained using a Quanta 250 microscope, FEI, USA. The UV-Vis absorption properties of the sodium titanate samples were obtained using a Lambda 35 spectrometer, PE, USA. An ASAP2460 porosity analyser, Micromeritics, USA. was used to study the surface area and porosity of the materials.

2.3. Activity of the sodium titanate photocatalysts

Ofloxacin was applied to study the activity of the sodium titanate samples. The photocatalyst was stirred in an ofloxacin solution (20 mg/L, 50 mL) in the dark for 30 min. Then the mixture was irradiated under a UV light (main photon wavelength 253.7 nm, 2,300 μW/cm^2). The ofloxacin concentration was determined using an Agilent 1260 liquid chromatography, Agilent, USA (C18 column; $V_{(1\% \text{ phosphoric acid})}$: $V_{(\text{acetonitrile})}$ = 80:20).

Table 1
Sodium titanate samples prepared with different n(Na)/n(Ti) ratios

Sample	n(Na)/n(Ti)
Na_2Ti_3	2:3
Na_2Ti_6	2:6
Na_2Ti_9	2:9

Hydroxyl radicals generated on the sodium titanate samples were identified using a 0.5 mmol/L terephthalic acid solution. 2-Hydroxyterephthalic acid was produced after 30 min of irradiation in the presence of the photocatalysts. The fluorescence spectra of the 2-hydroxyterephthalic acid solution were obtained using a fluorescence spectrophotometer (LS-55, excited at 315 nm).

3. Results and discussions

3.1. Compositions in the sodium titanate samples

Fig. 1 shows the X-ray diffraction (XRD) patterns for the sodium titanate samples with different n(Na)/n(Ti) ratios. The compositions of the sodium titanate samples depended on the n(Na)/n(Ti) ratios in the precursor. $Na_2Ti_6O_{13}$ was the main substance in all the samples. The diffraction pattens for $Na_2Ti_6O_{13}$ were in accordance with the pattern in JCPDS 73–1398, belonging to a rhombic system. The sample Na_2Ti_6 was mainly composed of $Na_2Ti_6O_{13}$, and other phases were hardly observed in the XRD pattern. Several diffraction peaks in the XRD pattern for Na_2Ti_3 were assigned to $Na_4Ti_5O_{12}$. The diffraction intensity of $Na_2Ti_6O_{13}$ in the pattern for Na_2Ti_3 was much weaker than that for Na_2Ti_6. Besides $Na_2Ti_6O_{13}$, rutile phase TiO_2 was a minor component in Na_2Ti_9. Titania might have a strong activity in the photocatalytic reaction, but the activity of rutile TiO_2 is usually weaker than the activity of anatase TiO_2. Phase composition is a very important factor that can affect the activity of a photocatalyst.

The lattice parameters and crystallite sizes of $Na_2Ti_6O_{13}$ in the sodium titanate samples were calculated using a Jade 5.0 software and the Scherrer formula, as listed in Table 2. The crystallite sizes were the average values for the (200), (110), (310) and (020) planes of $Na_2Ti_6O_{13}$ crystals. The lattice parameters and crystallite sizes of $Na_2Ti_6O_{13}$ in Na_2Ti_6 and Na_2Ti_9 did not have noticeable differences, while the values for Na_2Ti_3 were much smaller. The growth of $Na_2Ti_6O_{13}$ crystals in Na_2Ti_3 was limited due to high n(Na)/n(Ti) ratio. Titanium in the precursor was not sufficient for the formation of stochiometric $Na_2Ti_6O_{13}$ crystals. The precursor for
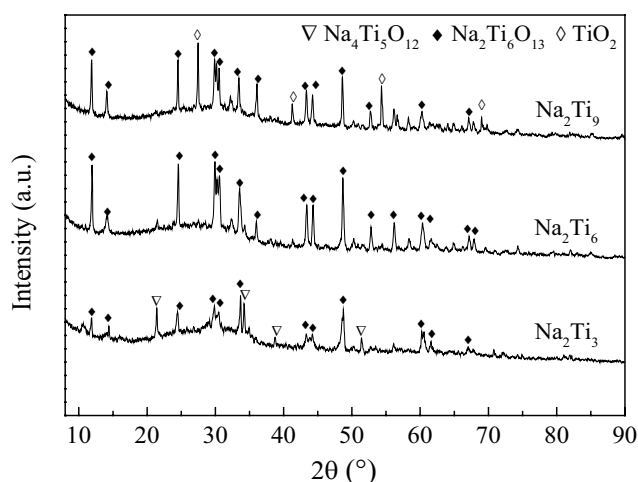
Fig. 1. X-ray diffraction patterns for the sodium titanates with different n(Na)/n(Ti) ratios.

Na_2Ti_9 had abundant titanium atoms. The excessive titanium atoms were converted into TiO_2 during calcination, but the formation of $Na_2Ti_6O_{13}$ crystals was not disturbed. Nanosized crystals usually have a stronger activity compared with large photocatalyst crystals.

3.2. Surface images of the sodium titanate samples

The surface images for the sodium titanate samples are shown in Fig. 2. The materials tended to form large particles during calcination. The aggregation tendency was very common for titanates prepared during high temperature thermal treatment. The big particles' size was as large as tens of micrometres. The sodium titanate samples were ground before characterizations, so there were many small fragments among the large particles.

3.3. Porosity characteristics

Fig. 3a presents the adsorption–desorption isotherms for the sodium titanate samples. Nitrogen was used as the adsorbate to determine the porosity of the materials. The adsorbed N_2 quantity on the sodium titanate samples was small when the relative nitrogen pressure was lower than 0.9. Capillary condensation of nitrogen at very high pressure led to the significant increase in the amount of the adsorbed nitrogen. The adsorption–desorption isotherms were regarded as an International Union of Pure and Applied Chemistry type IV isotherm, indicating the mesoporous structure in the materials. Fig. 3b presents the pore size distributions for the sodium titanate samples. The pores in the materials were mostly in the mesopore size range. The pore volumes in Na_2Ti_6 and Na_2Ti_9 were much larger than the pore volume in Na_2Ti_3.

Table 3 gives the porosity characteristics of the sodium titanate samples. The sodium titanates were a kind of mesoporous material, but the specific surface areas and pore volumes were not high. However, the specific surface areas and pore volumes for Na_2Ti_6 and Na_2Ti_9 were much larger than the values for Na_2Ti_3. Although the thermal treatment caused the avoidable aggregation tendency, the complete crystallization of $Na_2Ti_6O_{13}$ in Na_2Ti_6 and Na_2Ti_9 could enhance porosity in some extent. Since photocatalytic

Table 2
Lattice parameters and crystallite sizes of $Na_2Ti_6O_{13}$ in the sodium titanate samples

Sample	a (nm)	b (nm)	c (nm)	V (nm³)	Crystallite size (nm)
Na_2Ti_3	0.5297	0.5320	0.9537	0.2687	33.5
Na_2Ti_6	1.5045	0.3757	0.9202	0.5142	49.7
Na_2Ti_9	1.5071	0.3743	0.9140	0.5183	48.3
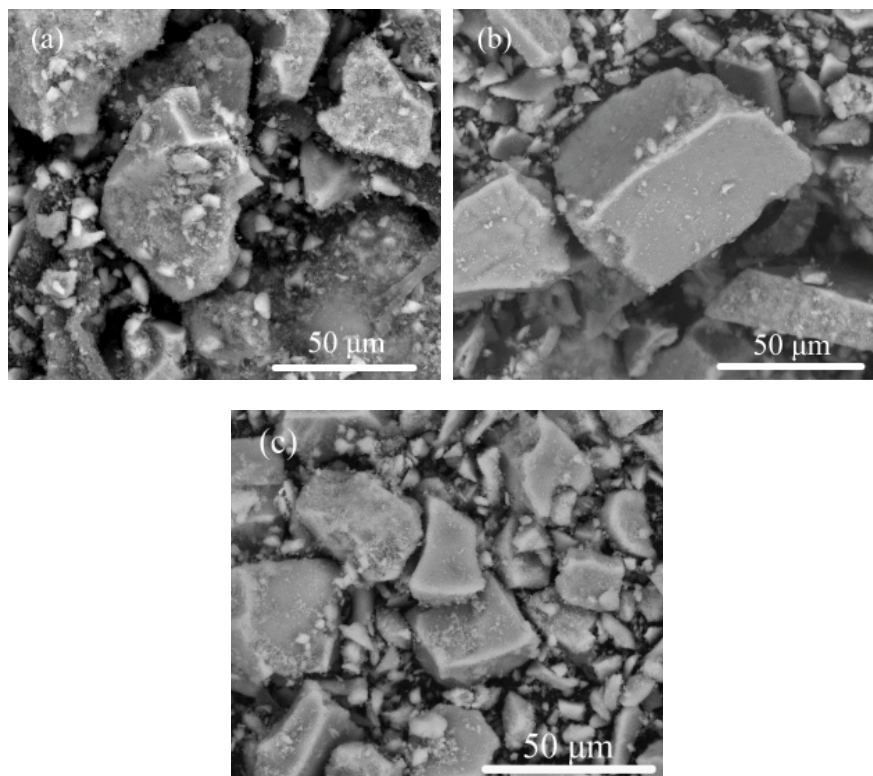
Fig. 2. Surface images for the sodium titanate samples.

reaction occurs on the surface of a photocatalyst, the surface area and porosity of the photocatalyst can greatly influence the activity. A material with large surface area usually has a strong activity on the degradation reaction.
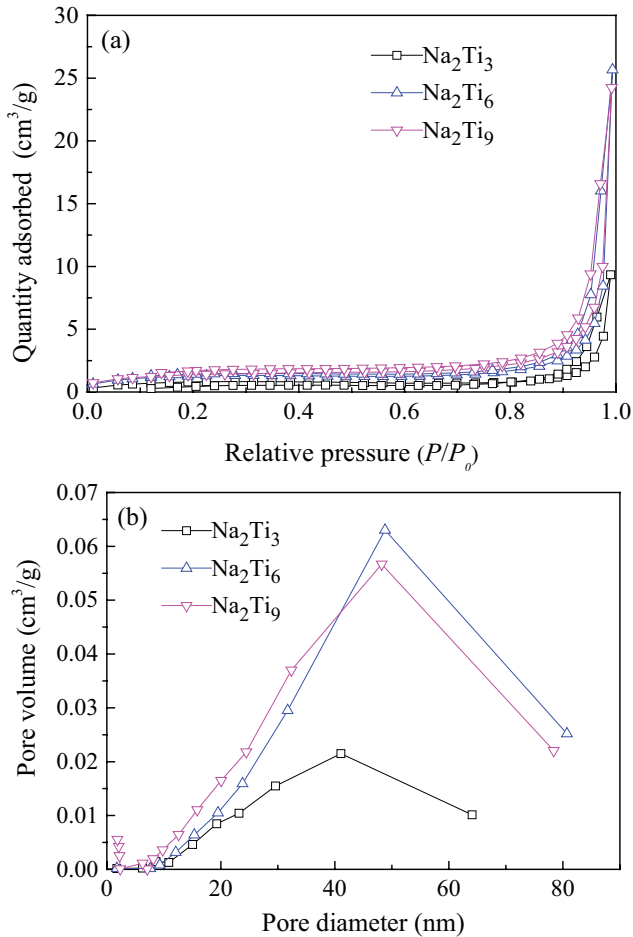
Fig. 3. (a) N_2 adsorption–desorption isotherms for the sodium titanate samples and (b) pore-size distributions in the sodium titanate samples.
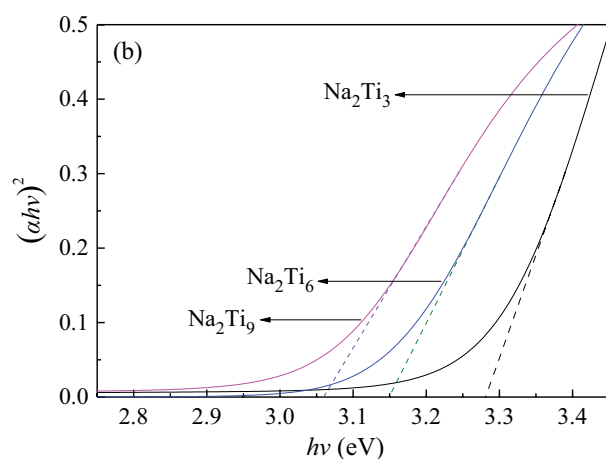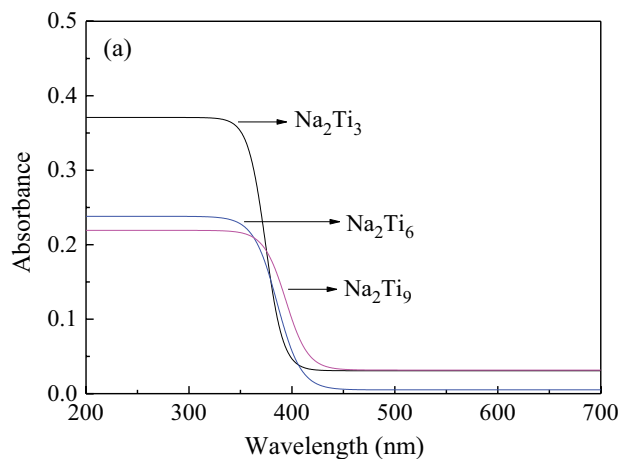
3.4. UV-Vis absorption and band gap energy

The UV-Vis absorption spectra for the sodium titanate samples are shown in Fig. 4a. The absorption spectra for the sodium titanates were mainly in the UV light region, while the band edges were very close to the ultraviolet-visible boundary. The materials could not absorb visible light energy to trigger the reaction. Based on the Tauc-plot method [25], the band gap energies of the sodium titanates were calculated using the hv–$(ahv)^2$ plots, as plotted in Fig. 4b. The band gap energies for Na_2Ti_3, Na_2Ti_6 and Na_2Ti_9 were calculated to be 3.28, 3.15 and 3.06 eV, respectively. The differences in the band gap energies for the sodium titanates were not significant. Such differences might be due to the phase composition and the crystal growth of $Na_2Ti_6O_{13}$ in the samples.

3.5. Hydroxyl radicals produced on the sodium titanates

The photocatalytic reaction was initiated by absorbing a photon if the photon energy was higher than the band gap energies of the sodium titanates. The photogenerated holes migrated to the surface of the materials, and the surface adsorbed OH groups were oxidized to produce hydroxyl radicals. The number of hydroxyl radicals produced on the materials was in a close correlation to the activity of the sodium titanates. Hydroxyl radicals generated on the sodium titanates were identified using a 0.5 mmol/L terephthalic acid solution. 2-Hydroxyterephthalic acid was produced under irradiation. Fig. 5 shows the fluorescence spectra of 2-hydroxyterephthalic acid solution after half

Table 3
Specific surface area, average pore size and pore volume of the sodium titanate samples

Sample	Specific surface area (m^2/g)	Average pore size (nm)	Pore volume (cm^3/g)
Na_2Ti_3	2.76	5.15	0.00361
Na_2Ti_6	4.29	6.74	0.00722
Na_2Ti_9	5.32	7.30	0.00970

Fig. 4. (a) UV-Vis absorption spectra for the sodium titanate samples and (b) hv–$(ahv)^2$ plots.

an hour of UV illumination in the presence of the sodium titanate samples. A higher fluorescence intensity means a stronger activity of the photocatalyst. The productivity of hydroxyl radical on the sodium titanates was in the sequence $Na_2Ti_9 > Na_2Ti_6 > Na_2Ti_3$. Hydroxyl radical is a major oxidative reagent in the photocatalytic reaction. The productivity of hydroxyl radical is greatly related to the activity of the material.

3.6. Ofloxacin degradation on the sodium titanates

Ofloxacin was adsorbed on the surface of the sodium titanates, followed by degradation under irradiation. As shown in Fig. 6, the proportion of ofloxacin molecules adsorbed on the materials was not more than 2%. The removal of ofloxacin from the solution depended on the activity of the sodium titanates. The ofloxacin degradation efficiencies after half an hour of reaction for Na_2Ti_3, Na_2Ti_6 and Na_2Ti_9

were obtained to be 30.1%, 47.9% and 53.5%, respectively. The activity of Na_2Ti_3 was much weaker than that of the other two materials, since the crystallization of $Na_2Ti_6O_{13}$ was not adequate in Na_2Ti_3.

The activity of Na_2Ti_9 was slightly stronger than the activity of Na_2Ti_6. This might be due to the difference in phase composition of the two materials. Na_2Ti_9 was composed of $Na_2Ti_6O_{13}$ and a small proportion of rutile TiO_2. It is hard to attribute the promoted activity to the existence of rutile TiO_2, since rutile TiO_2 usually has poor activity. As stated before, more hydroxyl radicals were produced on Na_2Ti_9 than that produced on Na_2Ti_6. The rutile TiO_2 might reduce the recombination of photogenerated electrons and holes, and then more hydroxyl radicals were generated.

Fig. 7a shows the concentration of ofloxacin solution during the photocatalytic process. The original ofloxacin molecules were nearly removed after 70 min of reaction in
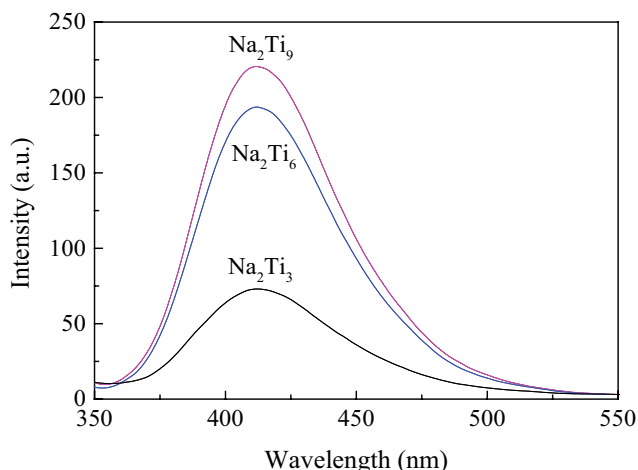
Fig. 5. Fluorescence spectra of 2-hydroxyterephthalic acid solution after 30 min of UV illumination in the presence of the sodium titanate samples.
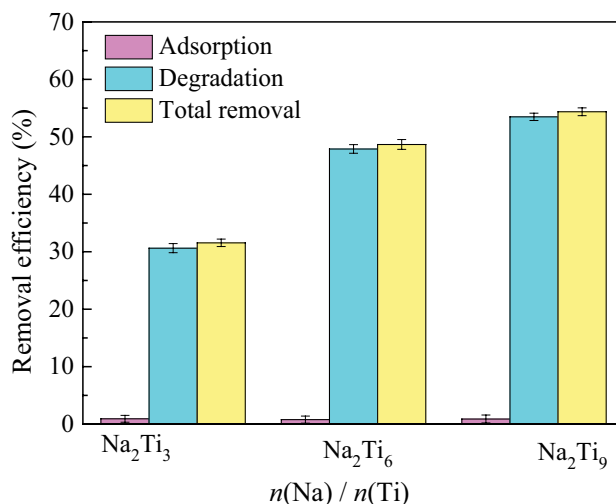
Fig. 6. Adsorption and photocatalytic degradation of ofloxacin on the sodium titanate samples. The irradiation time was 30 min.
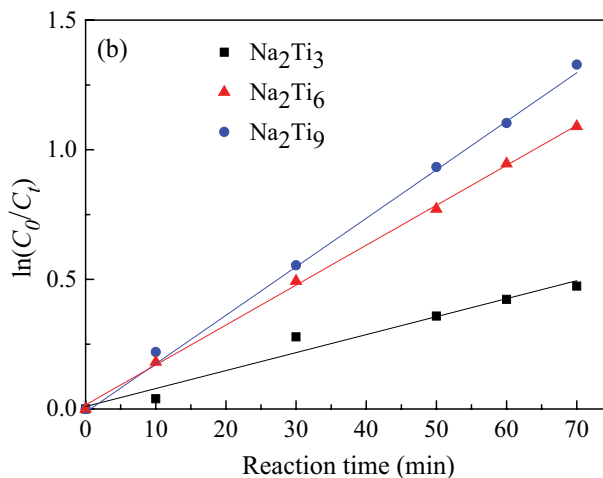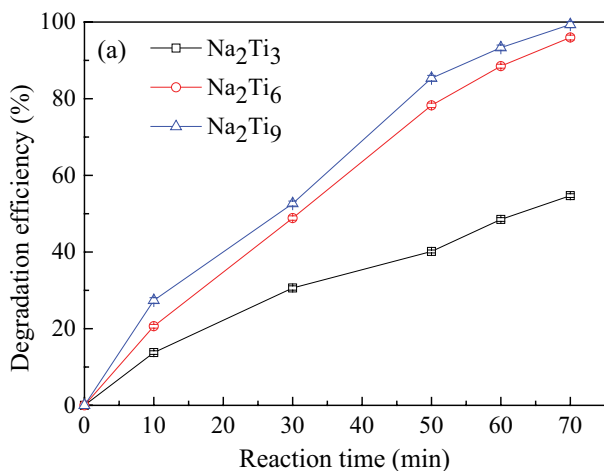
Fig. 7. (a) Photocatalytic degradation of ofloxacin with extended irradiation time and (b) kinetic plots for photocatalytic degradation of ofloxacin on the sodium titanate samples.
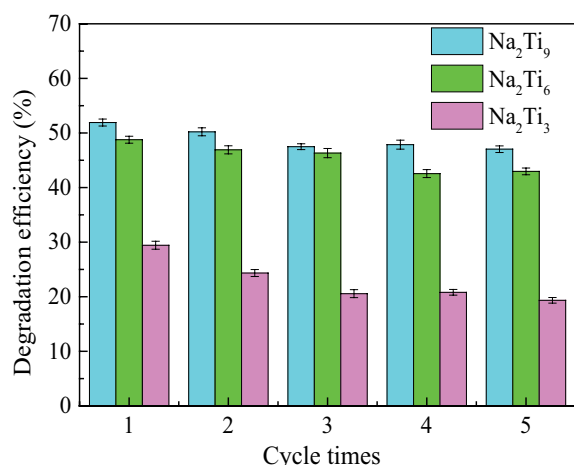
Fig. 8. Reusability of the sodium titanate samples for ofloxacin degradation.

the presence of Na_2Ti_6 and Na_2Ti_9, while the degradation efficiency was only 54.7% in the solution using Na_2Ti_3. The ofloxacin molecules could be fully removed during the oxidation process. Fig. 7b shows the first-order kinetic plots for the oxidation reactions. The reaction rate constants for ofloxacin degradation occurred on Na_2Ti_3, Na_2Ti_6 and Na_2Ti_9 were calculated to be 0.00693, 0.0154 and 0.0187 min^{-1}, respectively.

The photocatalyst needs to be reused in water treatment. Fig. 8 compares the reusability of the sodium titanates for ofloxacin degradation in 5 cycles. When the first cycle was finished after 30 min, a volume of 5 mL of the solution was used to examine the remaining ofloxacin concentration. Then another 5 mL of ofloxacin solution was added into the former solution to restore the initial ofloxacin solution (50 mL, 20 mg/L). The degradation efficiencies on Na_2Ti_6 and Na_2Ti_9 after the first cycle were 47.9% and 53.5%, respectively. A total of 88.1% of the original activity of Na_2Ti_6 was maintained in the fifth reaction cycle, and a total of 90.5% of the original activity of Na_2Ti_9 was maintained at the same time. The slight decrease in degradation efficiency was probably due to the removal of fine powders in the solution samples.

4. Conclusions

The influences of sodium/titanium molar ratio on the composition and properties of the sodium titanate samples were studied. The materials were mainly composed of $Na_2Ti_6O_{13}$, while $Na_4Ti_5O_{12}$ and rutile phase TiO_2 were the minor components in Na_2Ti_3 and Na_2Ti_9, respectively. The specific surface areas and pore volumes for Na_2Ti_6 and Na_2Ti_9 were much larger than the values for Na_2Ti_3. The absorption edges for the sodium titanates were very close to the ultraviolet-visible boundary. The productivity of hydroxyl radicals on the sodium titanates was in the sequence $Na_2Ti_9 > Na_2Ti_6 > Na_2Ti_3$. The proportion of ofloxacin molecules adsorbed on the materials was not more than 2%, and the ofloxacin molecules could be fully removed during the oxidation process. The sodium titanates had high activity even in the fifth reaction cycle to degrade ofloxacin.

References

[1] D. Barceló, B. Žonja, A. Ginebreda, Toxicity tests in wastewater and drinking water treatment processes: a complementary assessment tool to be on your radar, J. Environ. Chem. Eng., 8 (2020) 104262, doi: 10.1016/j.jece.2020.104262.

[2] H.B. Lu, Y. Yu, Y.X. Zhou, F. Xing, A quantitative evaluation method for wastewater toxicity based on a microbial fuel cell, Ecotoxicol. Environ. Saf., 183 (2019) 109589, doi: 10.1016/j.ecoenv.2019.109589.

[3] W.T. Zhao, Q. Sui, X. Huang, Removal and fate of polycyclic aromatic hydrocarbons in a hybrid anaerobic–anoxic–oxic process for highly toxic coke wastewater treatment, Sci. Total Environ., 635 (2018) 716–724.

[4] J. Zan, H. Song, S.Y. Zuo, X.R. Chen, D.S. Xia, D.Y. Li, MIL-53(Fe)-derived Fe_2O_3 with oxygen vacancy as Fenton-like photocatalysts for the elimination of toxic organics in wastewater, J. Cleaner Prod., 246 (2020) 118971, doi: 10.1016/j.jclepro.2019.118971.

[5] D.M. EL-Mekkawi, N.A. Abdelwahab, W.A.A. Mohamed, N.A. Taha, M.S.A. Abdel-Mottaleb, Solar photocatalytic treatment of industrial wastewater utilizing recycled polymeric disposals as TiO_2 supports, J. Cleaner Prod., 249 (2020) 119430, doi: 10.1016/j.jclepro.2019.119430.

[6] M. Martín-Sómer, C. Pablos, A. de Diego, R. van Grieken, Á. Encinas, V.M. Monsalvo, J. Marugán, Novel macroporous 3D photocatalytic foams for simultaneous wastewater disinfection and removal of contaminants of emerging concern, Chem. Eng. J., 366 (2019) 449–459.

[7] S.Y. Dong, L.F. Cui, W. Zhang, L.J. Xia, S.J. Zhou, C.K. Russell, M.H. Fan, J.L. Feng, J.H. Sun, Double-shelled $ZnSnO_3$ hollow cubes for efficient photocatalytic degradation of antibiotic wastewater, Chem. Eng. J., 384 (2020) 123279, doi: 10.1016/j.cej.2019.123279.

[8] G. Gupta, A. Umar, A. Kaur, S. Sood, A. Dhir, S.K. Kansal, Solar light driven photocatalytic degradation of ofloxacin based on ultra-thin bismuth molybdenum oxide nanosheets, Mater. Res. Bull., 99 (2018) 359–366.

[9] Z. Li, M. Qi, C. Tu, W. Wang, J. Chen, A.J. Wang, Highly efficient removal of chlorotetracycline from aqueous solution using graphene oxide/TiO_2 composite: properties and mechanism, Appl. Surf. Sci., 425 (2017) 765–775.

[10] Y. Hendrix, A. Lazaro, Q.L. Yu, H.J.H. Brouwers, Influence of synthesis conditions on the properties of photocatalytic titania-silica composites, J. Photochem. Photobiol., A, 371 (2019) 25–32.

[11] S. Deepracha, A. Ayral, M. Ogawa, Acceleration of the photocatalytic degradation of organics by *in-situ* removal of the products of degradation, Appl. Catal., B, 284 (2021) 119705, doi: 10.1016/j.apcatb.2020.119705.

[12] D.M. Tobaldi, D. Dvoranová, L. Lajaunie, N. Rozman, B. Figueiredo, M.P. Seabra, A. Sever Škapin, J.J. Calvino, V. Brezová, J.A. Labrincha, Graphene-TiO_2 hybrids for photocatalytic aided removal of VOCs and nitrogen oxides from outdoor environment, Chem. Eng. J., 405 (2021) 126651, doi: 10.1016/j.cej.2020.126651.

[13] B. Barrocas, L.D. Chiavassa, M. Conceição Oliveira, O.C. Monteiro, Impact of Fe, Mn co-doping in titanate nanowires photocatalytic performance for emergent organic pollutants removal, Chemosphere, 250 (2020) 126240, doi: 10.1016/j.chemosphere.2020.126240.

[14] J.X. Lu, D.L. Li, Y. Chai, L. Li, M. Li, Y.Y. Zhang, J. Liang, Rational design and preparation of nanoheterostructures based on zinc titanate for solar-driven photocatalytic conversion of CO_2 to valuable fuels, Appl. Catal., B, 256 (2019) 117800, doi: 10.1016/j.apcatb.2019.117800.

[15] S. Rahut, R. Panda, J.K. Basu, Solvothermal synthesis of a layered titanate nanosheets and its photocatalytic activity: effect of Ag doping, J. Photochem. Photobiol., A, 341 (2017) 12–19.

[16] G.G. Liu, K. Han, H.Q. Ye, C.Y. Zhu, Y.P. Gao, Y. Liu, Y.H. Zhou, Graphene oxide/triethanolamine modified titanate nanowires as photocatalytic membrane for water treatment, Chem. Eng. J., 320 (2017) 74–80.

[17] F. Tavasol, T. Tabatabaie, B. Ramavandi, F. Amiri, Design a new photocatalyst of sea sediment/titanate to remove cephalexin antibiotic from aqueous media in the presence of sonication/ ultraviolet/hydrogen peroxide: pathway and mechanism for degradation, Ultrason. Sonochem., 65 (2020) 105062, doi: 10.1016/j.ultsonch.2020.105062.

[18] W.W. Liu, Z.Q. Dai, Y. Liu, A.Q. Zhu, D.L. Zhong, J. Wang, J. Pan, Intimate contacted two-dimensional/zero-dimensional composite of bismuth titanate nanosheets supported ultrafine bismuth oxychloride nanoparticles for enhanced antibiotic residue degradation, J. Colloid Interface Sci., 529 (2018) 23–33.

[19] L.L. Yang, K.Q. Wang, J. Yang, W. Zhang, Role of hydrochloric acid treated HZSM-5 zeolite in $Sm_2Ti_2O_7$/nHZSM-5 composite for photocatalytic degradation of ofloxacin, J. Mater. Res. Technol., 9 (2020) 10585–10596.

[20] S. Madolappa, H.K. Choudhary, N. Punia, A.V. Anupama, B. Sahoo, Dielectric properties of A-site Mn-doped bismuth sodium titanate perovskite: $(Bi_{0.5}Na_{0.5})_{0.9}Mn_{0.1}TiO_3$, Mater. Chem. Phys., 270 (2021) 124849, doi: 10.1016/j.matchemphys.2021.124849.

[21] M. Esteves, L. Fernández-Werner, C.C.P. Cid, S. Pelegrini, A.A. Pasa, R. Faccio, Á.W. Mombrú, Optical, electrical and structural properties of Fe doped sodium titanate nanostructures, Appl. Surf. Sci., 552 (2021) 149534, doi: 10.1016/j.apsusc.2021.149534.

[22] Q.Q. Shi, A. Raza, L.L. Xu, G. Li, Bismuth oxyhalide quantum dots modified sodium titanate necklaces with exceptional population of oxygen vacancies and photocatalytic activity, J. Colloid Interface Sci., 625 (2022) 750–760.

[23] O. Shtyka, V. Shatsila, U. Novikau, R. Ciesielski, A. Kedziora, W. Maniukiewicz, T. Maniecki, Synthesis of mixed-phase sodium titanates and their activity in visible-light driven reduction of carbon dioxide, Catal. Commun., 168 (2022) 106462, doi: 10.1016/j.catcom.2022.106462.

[24] H.R. Wang, T. Sun, N. Xu, Q.Y. Zhou, L.M. Chang, 2D sodium titanate nanosheet encapsulated Ag_2O-TiO_2 *p-n* heterojunction photocatalyst: improving photocatalytic activity by the enhanced adsorption capacity, Ceram. Int., 47 (2021) 4905–4913.

[25] M.A. Butler, Photoelectrolysis and physical properties of the semiconducting electrode WO_2, J. Appl. Phys., 48 (1977) 1914–1920.